

Grokking at the Edge of Linear Separability

Alon Beck[†], Noam Levi[‡] & Yohai Bar Sinai[†]

[†]Raymond and Beverly Sackler School of Physics and Astronomy

Tel-Aviv University

Tel-Aviv 69978, Israel

[‡]École Polytechnique Fédérale de Lausanne (EPFL)

Switzerland

{alonbk2@gmail.com, noam.levi@epfl.ch, ybarsinai@gmail.com}

October 8, 2024

Abstract

We study the generalization properties of binary logistic classification in a simplified setting, for which a "memorizing" and "generalizing" solution can always be strictly defined, and elucidate empirically and analytically the mechanism underlying Grokking in its dynamics. We analyze the asymptotic long-time dynamics of logistic classification on a random feature model with a constant label and show that it exhibits Grokking, in the sense of delayed generalization and non-monotonic test loss. We find that Grokking is amplified when classification is applied to training sets which are on the verge of linear separability. Even though a perfect generalizing solution always exists, we prove the implicit bias of the logistic loss will cause the model to overfit if the training data is linearly separable from the origin. For training sets that are not separable from the origin, the model will always generalize perfectly asymptotically, but overfitting may occur at early stages of training. Importantly, in the vicinity of the transition, that is, for training sets that are almost separable from the origin, the model may overfit for arbitrarily long times before generalizing. We gain more insights by examining a tractable one-dimensional toy model that quantitatively captures the key features of the full model. Finally, we highlight intriguing common properties of our findings with recent literature, suggesting that grokking generally occurs in proximity to the interpolation threshold, reminiscent of critical phenomena often observed in physical systems.

1 Introduction

Understanding the relationship between the intrinsic properties of data, the training dynamics of neural networks (NNs), and their ability to generalize is crucial to explaining the success of modern machine learning (ML) algorithms. In particular, highly over-parameterized models based on the transformer architecture [Vaswani et al., 2023], such as Large Language Models (LLMs) [OpenAI, 2023, Google, 2023, Zeng et al., 2022, Brown et al., 2020, Chowdhery et al., 2022, Anil et al., 2023], as well as state of the art models for computer vision [Srivastava and Sharma, 2023], defy expectations and are able to generalize with a number of parameters far exceeding the so called interpolation threshold [Kaplan et al., 2020, Schaeffer et al., 2023]. Interestingly, these models have been shown to exhibit unpredictable behaviors when changing the number of network parameters, not only with respect to generalization, but also in their learning dynamics.

One such phenomenon is Grokking, first observed by [Power et al., 2022] when training a transformer model on modular arithmetic tasks. Grokking occurs when a model initially achieves perfect training accuracy but no generalization (i.e. no better than a random predictor), and upon further training, transitions to almost perfect generalization. This phenomenon has garnered substantial attention in recent years [Gromov, 2023, Liu et al., 2023, Xu et al., 2023] due to its striking contrast with naive expectations, whereby over-fitting is generally seen as an undesirable property of models that should not generalize with further training, originally dealt with using early stopping [Prechelt, 1996].

In this work, we study grokking in a synthetic, yet illuminating, setting where the asymptotic optimal solution can always be identified, allowing a sharp definition of notions which are typically

ambiguous, such as “memorization” and “learning”. Concretely, we focus on the extreme case of feature noise where the network needs to ignore the input features and classify all points as a constant label. The input data are N points in \mathbb{R}^d , drawn independently from an isotropic normal distribution with diagonal covariance, $\mathbf{x}_i \sim \mathcal{N}(0, \sigma \mathbf{I}_d)$ where \mathbf{I}_d is the $d \times d$ identity matrix and $\sigma > 0$. We study the limit of large $N, d \rightarrow \infty$, while keeping the ratio $\lambda = d/N$ fixed. Our main contributions are:

- We demonstrate both numerically and analytically that grokking may occur in this setting, and is promoted when λ is close to $1/2$ and σ is large.
- We demonstrate that this occurs because $\lambda = 1/2$ is the effective interpolation threshold, in the sense that for $\lambda < 1/2$ the model will almost surely asymptotically approach perfect generalization accuracy and vanishing loss. For $\lambda > 1/2$ the model will almost surely achieve imperfect generalization accuracy and the population loss will diverge at long times.
- We prove that the generalization properties depend only on whether the training set is linearly separable from the origin. The model will achieve asymptotically optimal generalization if and only if the origin is contained in the convex hull of the training set.
- Moreover, we show that near the threshold value, the dynamics may generically track the overfitting solution for arbitrarily long times before transitioning to the optimal generalizing solution, manifesting as non-monotonicity of the test loss and delayed generalization.
- We construct a simple, one-dimensional model which captures the salient aspects of the problem, and explicitly solve the time evolution of the network parameters for several interesting cases.

The main takeaway from our setup is that grokking happens near critical points in long-term dynamics, similar to the phenomenon known in the physics literature as ‘critical slowing down’. While further study is needed, we believe this applies to other grokking examples (see for example [Levi et al., 2023, Liu et al., 2023, Gromov, 2023]).

2 Related Work

Following the discovery of grokking by Power et al. [2022], numerous studies have attempted to elucidate its underlying mechanisms. Liu et al. [2022] showed that when sufficient data determines the structured representation, perfect generalization can be achieved on a non-modular addition task. Other works have identified factors contributing to grokking [Davies et al., 2023, Nanda et al., 2023], analyzed the trigonometric algorithms learned by networks after grokking [Nanda et al., 2023, Chughtai et al., 2023, Merrill et al., 2023, Gromov, 2023], and demonstrated similar dynamics in sparse parity tasks [Merrill et al., 2023]. Additional works proposed “slingshots” [Thilak et al., 2022] or “oscillations” [Notsawo et al., 2023] as explanations for grokking, while others have studied the role of regularization, which has proven to significantly impact grokking in certain scenarios [Power et al., 2022, Liu et al., 2023]. Our work requires none of these in order to exhibit or explain grokking.

Recently, a body of works on solvable models which grok in various settings has emerged. Liu et al. [2023], Kumar et al. [2023] and Lyu et al. [2024] have linked grokking to memorization and transitions from lazy to rich dynamics. Žunkovič and Ilievski [2022], Gromov [2023], Doshi et al. [2024] analyzed solvable models exhibiting grokking and related their findings to the formation of latent-space structure, Xu et al. [2023] related grokking to benign over-fitting for ReLU networks on XOR data, Rubin et al. [2024] described grokking as a first-order phase transition, and Levi et al. [2023] provide the full dynamical solution of grokking in linear regression. Our work attempts to fill the gap between solvable models and representation learning, whereby we can always identify the optimal solutions, while still solving the dynamics of the model. To accomplish this, our work relies heavily on the results of Soudry et al. [2018], Nacson et al. [2019], Ji and Telgarsky [2019], which analyze the late-time dynamics properties of logistic regression for separable and inseparable data under gradient descent (GD).

3 Grokking in Binary Classification

3.1 Model Setup and Empirical Results

We will now define the setup of the model performing binary classification using logistic regression and present the numerical evidence for grokking. Consider a dataset of N training samples $\mathbf{x}_i \in \mathbb{R}^d$ which are identically and independently distributed (iid) vectors, $\mathbf{x}_i \sim \mathcal{N}(0, \sigma^2 \mathbf{I}_d)$ with $\sigma > 0$ the feature standard deviation, and \mathbf{I}_d is the $d \times d$ identity matrix. The task is logistic classification, where all input points are assigned the same label. We work in the $N, d \rightarrow \infty$ regime, and their ratio, $\lambda = d/N$, plays a crucial role in the network’s training dynamics and generalization properties.

The network parameters consist of a weight vector $\mathbf{S} \in \mathbb{R}^d$ and a bias term $b \in \mathbb{R}$ and the network output is a scalar $f(\mathbf{x}_i) = \mathbf{S} \cdot \mathbf{x}_i + b$. We optimize the cross-entropy loss, given by

$$\mathcal{L}(\mathbf{S}, b) = \frac{1}{N} \sum_{i=1}^N \ell(\mathbf{S}^T \mathbf{x}_i + b) \ , \quad \ell(f) = \log(1 + e^f) \ . \quad (1)$$

We define the empirical accuracy over the dataset as

$$\mathcal{A} = \frac{1}{N} \sum_{i=1}^N \Theta(-\mathbf{S}^T \mathbf{x}_i - b) \ , \quad (2)$$

where $\Theta(z)$ is the Heaviside function. The GD equations at training step t with learning rate η are

$$\mathbf{S}_{t+1} - \mathbf{S}_t = -\eta \nabla_{\mathbf{S}} \mathcal{L}, \quad b_{t+1} - b_t = -\eta \partial_b \mathcal{L}. \quad (3)$$

In this paper we will focus primarily on the gradient flow limit ($\eta \rightarrow 0$) of these equations. In Fig. 1 we show numerical results depicting the gradient-descent dynamics of the model across three values of $\lambda \equiv d/N$. Notably, we observe a significant grokking effect, both in the non-monotonicity of the test loss, and the delayed increase in test accuracy, only when λ approaches $\lambda_c = 1/2$ (there may be some differences between the grokking observed here and other examples in the literature, but they seem to be superficial - see Appendix B). In the following section, we explain how λ_c can be interpreted as the interpolation threshold in this setting.

3.2 The Mechanism of Grokking in the Current Setting

We begin by examining the optimal generalizing solution, that indicates the network has properly learned the task. Since the support of the input distribution is unbounded, the network should put all points in \mathbb{R}^d on the same side of the separating hyperplane, or in other words, push the decision boundary to infinity.

To see this rigorously, we derive expressions for the generalization accuracy and loss. Since the data is Gaussian, $x_i \sim \mathcal{N}(0, \sigma^2 \mathbf{I}_d)$, the generalization (population) loss is, by definition,

$$\mathcal{L}_{\text{gen}} = \mathbb{E}_{\mathbf{x} \sim \mathcal{N}(0, \sigma^2 \mathbf{I}_d)} [\log(1 + \exp(\mathbf{S}^T \mathbf{x} + b))] \ . \quad (4)$$

Since $\mathbf{S}^T \mathbf{x}$ is a linear combination of normal variables, it is normally distributed with zero mean and variance $\mathbb{E}[(\mathbf{S}^T \mathbf{x})^2] = \|\mathbf{S}\|^2 \sigma^2$, allowing us to perform a change of variables on Eq. (4), simplifying it to

$$\mathcal{L}_{\text{gen}} = \mathbb{E}_{y \sim \mathcal{N}(0,1)} \left[\log \left(1 + e^{\sigma \|\mathbf{S}\| y + b} \right) \right] \ . \quad (5)$$

Note that \mathcal{L}_{gen} is a function of b and $\|\mathbf{S}\|$ only. Similarly, the accuracy is given by

$$\mathcal{A}_{\text{gen}}(\mathbf{S}, b) = \mathbb{E}_{y \sim \mathcal{N}(0,1)} \left[\Theta(-\sigma \|\mathbf{S}\| y - b) \right] = \frac{1}{2} \left[1 - \text{erf} \left(\frac{1}{\sqrt{2}} \frac{b}{\sigma \|\mathbf{S}\|} \right) \right] \ . \quad (6)$$

In passing, we note that following the same procedure to obtain analogous expressions for the training loss and accuracy will not work. As discussed below, the training dynamics drive \mathbf{S} towards a value that depends on the training set, and hence the distribution of $\mathbf{S}^T \mathbf{x}$ on the training set deviates significantly from Gaussianity, see Fig. 2.

Examining these results, we see that indeed perfect generalization, i.e. $\mathcal{L} \rightarrow 0$, $\mathcal{A} \rightarrow 1$, is achieved only for $b \rightarrow -\infty$ and $b/\|\mathbf{S}\| \rightarrow -\infty$, i.e., b must tend to negative infinity while also being infinitely large compared to $\|\mathbf{S}\|$.

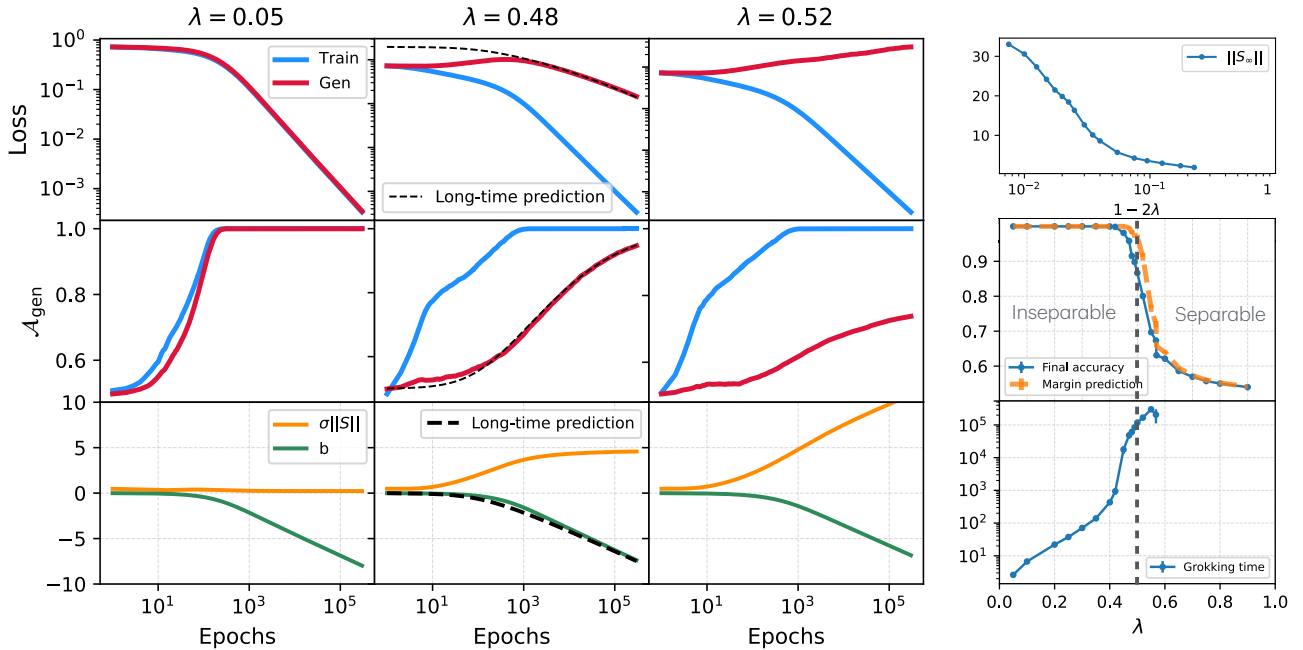


Figure 1: **Left panels: Gradient descent dynamics for three different values of $\lambda = d/N$.** In the *top row* and *middle row*, we show the loss and accuracy for the train and test datasets, while in the *bottom row*, we present the evolution of $b(t)$ and $\|\mathbf{S}(t)\|$. Grokking is significant only when λ approaches to 0.5 from below. We can see that for $\lambda > 0.5$, $\|\mathbf{S}\|$ increase indefinitely and generalization is not possible (see Eq. (6)). The parameters are $N = 4 \cdot 10^4$, $\sigma = 5$, $\eta = 0.01$. The direction of $\mathbf{S}(t=0)$ was drawn isotropically with $\|\mathbf{S}_0\| = 0.1$ and $b(t=0) = 0$. The number of test samples is $N_{\text{test}} = 10^4$. **Right panels:** Top: The norm of the limiting value \mathbf{S}_∞ in the separable case $\lambda > 1/2$, as a function of λ . Note that $\|\mathbf{S}_\infty\|$ diverges for $\lambda \rightarrow \frac{1}{2}$. Middle: the accuracy at the end of the training (in blue), and the predicted limiting accuracy (orange), calculated only using the margin of the dataset, see Eq. (13). Bottom: The Grokking time, defined practically as the delay between the times where the training and generalization accuracy surpass a threshold of 0.9, versus λ . We can see that the Grokking time and $\|\mathbf{S}_\infty\|$ diverge near $\lambda = 0.5$. Additional details regarding the experiments can be found in Appendix H.

Indeed, the bottom panels of Fig. 1 show that the behavior of b tends to $-\infty$ at late times in all parameter regimes. However, while $\|\mathbf{S}\|$ saturates on a constant for $\lambda < 1/2$, it goes to ∞ at long times for $\lambda > 1/2$, and does so at a rate comparable to b , leading to sub-optimal generalization $\lim_{t \rightarrow \infty} \mathcal{A}(\mathbf{S}(t), b(t)) < 1$.

These results are closely related to the framework developed by [Soudry et al., 2018], who studied the convergence of binary classification for linearly separable data, and later expanded by [Ji and Telgarsky, 2019] for inseparable data. In our case, since the model contains a bias term and all labels are the same, the data is always separable by a hyperplane “at infinity”. To use their framework, we need to work in an extended space of dimension $d + 1$, where we define the extended weight vector $\mathbf{w} = (\mathbf{S}, b) \in \mathbb{R}^{d+1}$. A direct corollary of Theorem 3 from [Soudry et al., 2018] is that at long times, the training dynamics behave as

$$\mathbf{w}(t) = \mathbf{w}_{\text{SVM}} \log(t) + \boldsymbol{\rho}(t), \quad \mathbf{w}_{\text{SVM}} = \underset{(\mathbf{S}, b)}{\operatorname{argmin}} \left\{ \|\mathbf{S}\|^2 + b^2 \quad \text{s.t.} \quad \mathbf{S}^T \mathbf{x}_i + b \leq -1 \right\}. \quad (7)$$

Here, \mathbf{w}_{SVM} is the solution¹ to the hard margin SVM problem in the extended $d + 1$ space and $\boldsymbol{\rho}$ is a residual vector which is bounded for all t .

Connecting this result to the previous discussion, we see indeed that either $|b|$ and/or $\|\mathbf{S}\|$ must diverge at long times, and the question is now reduced to what is the direction of \mathbf{w}_{SVM} . The true generalizing solution, which classifies correctly all points in \mathbb{R}^d is when $\mathbf{w}_{\text{SVM}} = (0, -1)$, i.e. when it points in the direction of the bias and the separating plane is at infinity. This is exactly the

¹Note that the SVM solution in the extended $d + 1$ is not the same as the typical formulation of the Support Vector Machine (SVM) with bias in d dimensions, because of the different penalty used for the bias term.

aforementioned condition $b \rightarrow -\infty$ and $|b|/\|\mathbf{S}\| \rightarrow \infty$. Overfitting occurs when the hyperplane is only far enough from the data to correctly classify all the training samples. In the extended space, this means that \mathbf{w}_{SVM} also contains a component in the direction of the data, and the model did not learn correctly the data distribution.

We are now ready to sketch our main claims regarding the grokking phenomenology presented in Fig. 1. The details will be fleshed out in the next subsections. We claim that:

- The generalization and overfitting at long times depend only on whether the training samples (in \mathbb{R}^d) are linearly separable from the origin. We call a training set *separable* if there exists a vector \mathbf{S} such that $\forall i \mathbf{S}^T \mathbf{x}_i < -1$, and *inseparable* otherwise.
- In the limit of large N, d , the training set is almost surely separable (inseparable) for $\lambda > \frac{1}{2}$ ($\lambda < \frac{1}{2}$). This is a direct corollary of Wendel’s theorem, [Wendel, 1962], see App. A for additional details.
- For separable training sets ($\lambda > \frac{1}{2}$), the model will always overfit, and the limiting generalization accuracy is directly related to the optimal separating margin. For inseparable training sets ($\lambda < \frac{1}{2}$) the model will always generalize perfectly: b diverges at long times and \mathbf{S} saturates on a finite value $\lim_{t \rightarrow \infty} \mathbf{S}(t) = \mathbf{S}_\infty$. This is shown in Sec. 3.3.
- However, for $\lambda \lesssim \frac{1}{2}$, the training set is on the verge of separability, and $\|\mathbf{S}_\infty\|$ may be arbitrarily large. Consequently, dynamics may take arbitrarily long times to reach the generalizing solution. This is the underlying mechanism of grokking in this setting.

3.3 Overfitting and Linear Separability

When will over-fitting occur? Due to the “exponential tail” of the cross-entropy loss, at late times the loss is dominated by samples with large network outputs $f = \mathbf{S}^T \mathbf{x} + b$, for which the cross-entropy loss $\ell(f)$ of Eq. (1), approaches the exponential loss $\ell_e(f) = e^f$ [Soudry et al., 2018, Nacson et al., 2019]. Specifically, the exponential loss will converge to the same late time dynamics as the cross entropy loss. Therefore, we will consider the exponential loss for which the calculations are tractable,

$$\mathcal{L}_e(\mathbf{S}, b) = \frac{1}{N} \sum_{i=1}^N e^{\mathbf{S}^T \mathbf{x}_i + b}. \quad (8)$$

In the gradient-flow limit, the dynamics for the exponential loss are

$$\frac{\partial \mathbf{S}}{\partial t} = -\frac{\eta}{N} e^b \sum_i e^{\mathbf{S}^T \mathbf{x}_i} \mathbf{x}_i, \quad \frac{\partial b}{\partial t} = -\frac{\eta}{N} e^b \sum_i e^{\mathbf{S}^T \mathbf{x}_i}. \quad (9)$$

Note that both rates are proportional to a common time-dependent scalar $e^{b(t)}$. Therefore one can define a so-called “conformal time”: $\tau(t) = \int_0^t e^{b(t')} dt'$, which is a common measure in cosmology and gravitational physics to describe co-moving objects in an expanding or shrinking spacetime background [Guth, 1981]. In terms of τ , the equations become

$$\frac{\partial \mathbf{S}}{\partial \tau} = -\frac{\eta}{N} \sum_i e^{\mathbf{S}^T \mathbf{x}_i} \mathbf{x}_i, \quad \frac{\partial b}{\partial \tau} = -\frac{\eta}{N} \sum_i e^{\mathbf{S}^T \mathbf{x}_i}. \quad (10)$$

The importance of this result is that the dynamics of $\mathbf{S}(\tau)$ in terms of the conformal time are identical to those of $\mathbf{S}(t)$ *in the absence of bias*. That is, $\mathbf{S}(t)$ follows the same path that would be obtained by minimizing $\mathcal{L} = \frac{1}{N} \sum_{i=1}^N e^{\mathbf{S}^T \mathbf{x}_i}$, but does so at a different rate which depends exponentially on the current value of $b(t)$. This is demonstrated in the middle panel of Fig. 2. Since $\tau(t)$ diverges for $t \rightarrow \infty$, $\mathbf{S}(t)$ must follow the same path at long times, as it would have followed without bias (see App. C for details).

Inseparable training set Using this result, let us consider the dynamics without bias. In the case where the data is not separable, \mathcal{L}_e of Eq. (8) is unbounded in all directions. That is, for any unit vector $\mathbf{e} \in \mathbb{R}^d$ s.t. $\|\mathbf{e}\| = 1$ we have $\lim_{\alpha \rightarrow \infty} \mathcal{L}_e(\alpha \mathbf{e}, 0) = \infty$. Since \mathcal{L}_e is convex, the gradient flow dynamics will lead to a global minimum at a finite point $\lim_{t \rightarrow \infty} \mathbf{S}(t) = \mathbf{S}_\infty$. From Eq. (7), we know that either

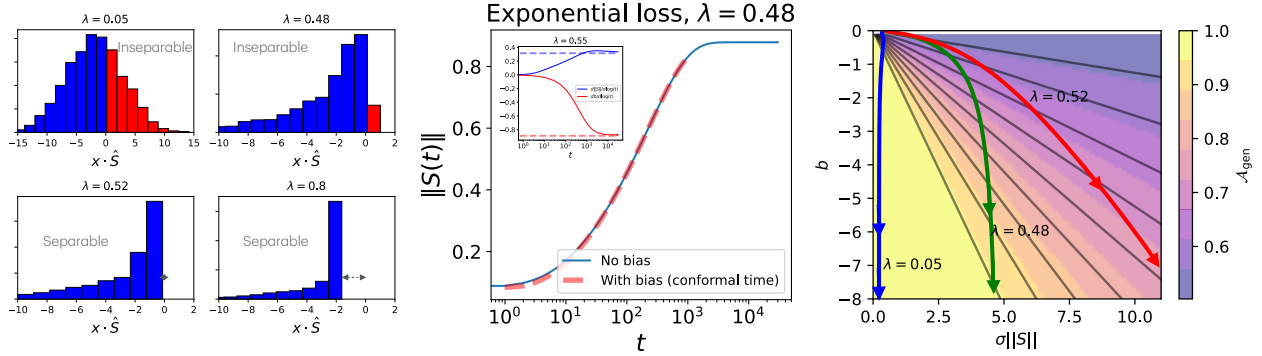


Figure 2: **Evolution of the network parameters.** In the *left* panel, we show the distribution of $\mathbf{S}^T \mathbf{x}_i / \|\mathbf{S}\|$, where $\mathbf{S} = \mathbf{S}(t_{\text{end}})$ is the final spatial weight vector that was found using GD dynamics for $\lambda = 0.05, 0.48, 0.52, 0.8$. The parameters are identical to those of Fig. 1. We can see that for $\lambda = 0.05, 0.48$ the model is not separable, while for $0.52, 0.8$ it is. For $\lambda = 0.8$, the distance of the distribution from 0 is the margin, indicated by the dashed two-sided arrow. *Middle* panel: $\|\mathbf{S}(t)\|$, optimized with GD using the exponential loss given in Eq. (8), with and without a bias term. With a bias term, the result is shown as a function of the conformal time $\tau = \int_0^t e^{b(t')} dt'$, and we can indeed see that it follows the same path but at a different rate. In the *inset*, we show the numerical calculation of $\frac{d\|\mathbf{S}\|}{d\log(t)}$ and $\frac{db}{d\log(t)}$, and the expected limiting values given in Eq. (12). *Right* panel: Optimization paths for different λ values, shown in the $b, \sigma\|\mathbf{S}\|$ plane. We see that for inseparable data, only b diverges along the path, while slightly above the verge of separability, both $b, \sigma\|\mathbf{S}\|$ diverge, leading to sub-optimal generalization accuracy.

$\|\mathbf{S}(t)\|$ or $|b(t)|$ must diverge, and since $\mathbf{S}(t)$ approaches a finite value, we conclude that $|b|/\|\mathbf{S}\| \rightarrow \infty$ at long times. That is, $\mathbf{w}_{\text{SVM}} = (0, -1)$ and the model flows towards the generalizing solution.

Separable training set For the separable case, it is easier to examine the optimization problem in Eq. (7) directly. We wish to minimize $\|\mathbf{w}\|^2 = \|\mathbf{S}\|^2 + b^2$ under the separability constraints. The generalizing solution $\mathbf{w}_g = (0, -1)$ satisfies all constraints trivially and has $\|\mathbf{w}_g\| = 1$. However, since the data is separable, there exists another solution to the constraints, namely $\mathbf{w}^* = (\mathbf{S}^*, 0)$, where \mathbf{S}^* is the separating vector in d dimensions without bias, i.e. the solution to

$$\mathbf{S}^* = \underset{\mathbf{S}}{\text{argmin}} \left\{ \|\mathbf{S}\|^2 \quad \text{s.t.} \quad \mathbf{S}^T \mathbf{x}_i \leq -1 \right\}. \quad (11)$$

The norm of \mathbf{S}^* is the inverse of the separation margin $M = 1/\|\mathbf{S}^*\|$.

Due to convexity, any convex combination of the form $\alpha \mathbf{w}_g + (1 - \alpha) \mathbf{w}^*$ with $0 < \alpha < 1$ also satisfies the constraints, and since they are orthogonal, it also has a smaller norm. The combination with the smallest norm is the global optimum, which is easily shown to be

$$\mathbf{w}_{\text{SVM}} = \frac{1}{1 + M^2} (M^2 \mathbf{S}^*, -1). \quad (12)$$

That is, for long times both \mathbf{S} and b diverge, and we have

$$\lim_{t \rightarrow \infty} \frac{b(t)}{\|\mathbf{S}(t)\|} = -\frac{1}{M}, \quad \lim_{t \rightarrow \infty} \mathcal{A}_{\text{gen}} = \frac{1}{2} \left[1 + \text{erf} \left(\frac{1}{\sigma M \sqrt{2}} \right) \right]. \quad (13)$$

This is also verified by an independent calculation in App. G, and is demonstrated numerically in the inset of the middle panel of Fig. 2. Finally, it can be shown directly from Eq. (5) that in this case the generalization loss diverges. In Fig. 2, we present the distribution of $\mathbf{S}^T \mathbf{x}_i / \|\mathbf{S}\|$ after training with GD, for various values of λ . We can see that for $\lambda < 1/2$ the dataset is inseparable, while it becomes separable for $\lambda > 1/2$.

3.4 When Will We See Grokking?

We have established that for inseparable sets $\mathbf{S}(t)$ flows to a fixed point \mathbf{S}_∞ while for separable sets it diverges at long times. This drastic change in the asymptotic value is responsible for grokking,

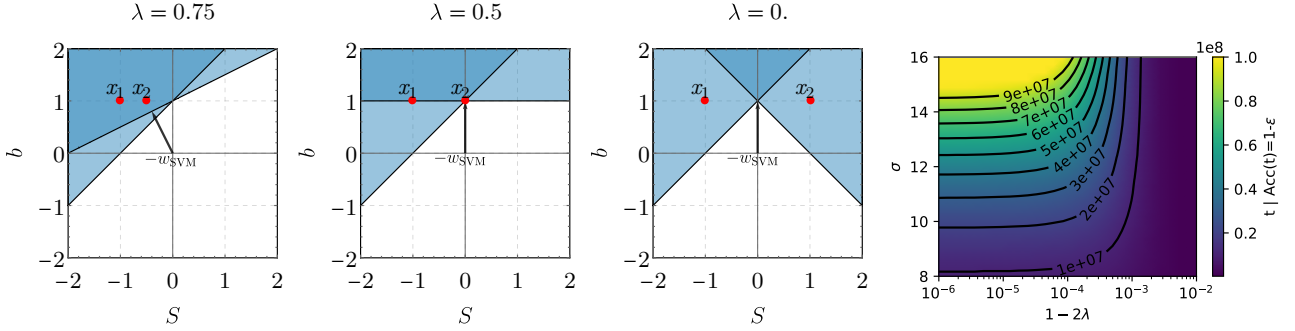


Figure 3: **Illustration of the SVM solutions for the effective simplified model.** The left panels: Illustration of how to find the hard margin SVM vector in 1+1 dimensions in the simplified model. For $\lambda < 0.5$, we have $w_{\text{SVM}} = (0, -1)$ while for $\lambda > 0.5$ we have $w_{\text{SVM}} = \left(\frac{M}{1+M^2}, -\frac{1}{1+M^2} \right)$, where the margin is $M = 2\lambda - 1$. We note that finding $-w_{\text{SVM}}$ is equivalent to finding the minimum vector that is in the intersection of the two regions determined by $w_{\text{SVM}}^T x_i \leq -1$. Right panel: The grokking time, defined as the time it takes for the generalization accuracy to reach 0.95, is plotted against σ and $1 - 2\lambda$. We see it diverges only in the limits of $\lambda \rightarrow 0.5$ and $\sigma \rightarrow \infty$ (neither of these conditions alone suffices to cause divergence).

much like in [Rubin et al., 2024] and [Levi et al., 2023], who showed that grokking occurs near a phase transition.

The manifestation of this discontinuity in our setting is that $\|\mathbf{S}_\infty\|$ diverges when the training set is almost separable. This statement is formally proven in App. D and empirically demonstrated in Fig. 1. It can also be obtained as a corollary of [Ji and Telgarsky, 2019].

To see this intuitively, consider a training set which is only slightly inseparable from the origin, i.e. one can make it separable by translating all points by a small amount. Since the set is inseparable, we asymptotically have $\mathbf{S}(t) \rightarrow \mathbf{S}_\infty$. However, on the translated points, $\|\mathbf{S}(t)\| \rightarrow \infty$. Since the solution to the gradient flow equations is smooth in the position of the training points, we must have that $\|\mathbf{S}_\infty\|$ is large.

Grokking occurs when the dynamics first follow the path towards \mathbf{S}_∞ , which is large but finite, while b remains small, and only then transition into the generalizing solution $b \rightarrow -\infty$. In this case we will see small values of $|b| / \|\mathbf{S}(t)\|$ at intermediate times and therefore delayed generalization. However, the dynamics may also flow along a different path in which $\mathbf{S}(t)$ and $b(t)$ grow at a comparable rate. Here, we show that grokking occurs generically when σ is large enough.

To see this, it useful to define the rescaled variables $\tilde{\mathbf{x}}_i = \mathbf{x}_i / \sigma$, $\tilde{\mathbf{S}} = \sigma \mathbf{S}$. Clearly, $\tilde{\mathbf{x}}_i \sim \mathcal{N}(0, \mathbf{I}_d)$. The gradient flow equations in terms of the rescaled variables are (we study the exponential loss here for simplicity)

$$\frac{\partial \tilde{\mathbf{S}}}{\partial t} = -\sigma^2 \frac{\eta}{N} e^b \sum_i e^{\tilde{\mathbf{S}}^T \tilde{\mathbf{x}}_i} \tilde{\mathbf{x}}_i, \quad \frac{\partial b}{\partial t} = -\frac{\eta}{N} e^b \sum_i e^{\tilde{\mathbf{S}}^T \tilde{\mathbf{x}}_i}. \quad (14)$$

Note that these are identical to the gradient flow equations of the original variables, Eq. (9) but the dynamics of \mathbf{S} are *faster* by factor of σ^2 . Thus, by taking a large σ , $\tilde{\mathbf{S}}$ will approach its asymptotic value \mathbf{S}_∞ arbitrarily fast, while the dynamics b will not change. Therefore, for large σ and large \mathbf{S}_∞ , we expect to see delayed generalization. The ‘‘Grokking time’’, i.e. the difference between the times for which training and generalization accuracy surpass a threshold, can truly diverge only if *both* $\lambda \rightarrow 0.5$ and $\sigma \rightarrow \infty$. This is also demonstrated for the simplified model (discussed below), see the right-most panel of Fig. 3.

Interestingly, using adaptive momentum based optimizers like ADAM [Kingma and Ba, 2017], one can see grokking even for $\sigma = 1$: Since these optimizers use a different learning rate for each parameter, based on historical gradients, this can lead to faster convergence in the direction of \mathbf{S} , enabling grokking for a similar reason as increasing σ . For elaboration, and discussion of the (similar) effect of initial conditions, see App. F.

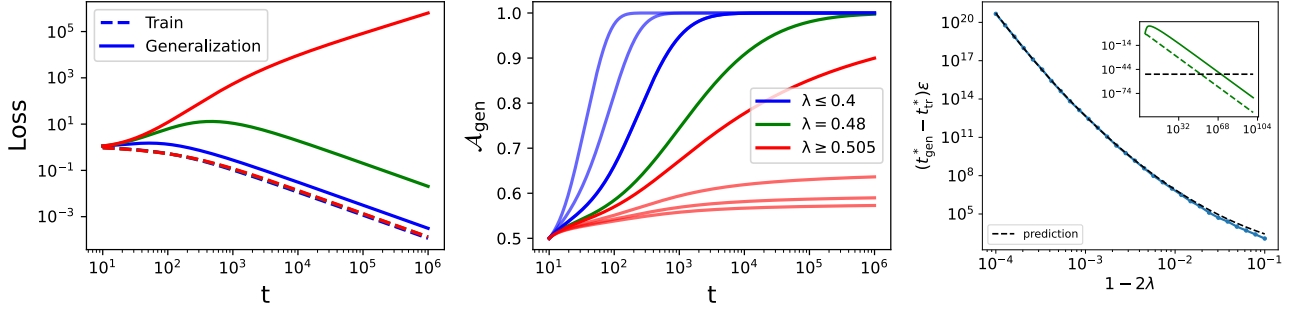


Figure 4: In the left panel, we calculate the loss and accuracy for different λ and $\sigma = 5$ in the simplified model (dotted/solid lines represent the training/generalization respectively). In the right panel, we plot the Grokking time (the time difference between the time it takes for the training and generalization loss to reach a certain threshold, $\varepsilon = 10^{-50}$ in this case) for $\sigma = 20$ and see that it is in very good agreement with the prediction. In the inset, we demonstrate how the grokking time is calculated for $\varepsilon = 10^{-50}$ and $\lambda = 10^{-4}$.

4 Insights From a Simplified Model

Our main claim is that the asymptotic dynamics depend only on the separability of the training set, and that grokking occurs at the edge of linear separability. This intuition works also at low dimensions, which are easier to understand.

Consider the case of $d = 1$. In this case, separability boils down to asking whether the origin is contained between the extremal points $\min\{x_i\}$ and $\max\{x_i\}$. Therefore, all the phenomenology of the full model described in the previous sections can be captured by a training set consisting of only 2 points x_1, x_2 . For consistency with the problem of Gaussian data, we parameterize this set as

$$x_1 = -\sigma, \quad x_2 = \sigma(1 - 2\lambda), \quad \mathcal{L}(S, b) = \frac{1}{2} \left(e^{Sx_1+b} + e^{Sx_2+b} \right), \quad (15)$$

so that the scale of x_i is σ , and they are separable (inseparable) for $\lambda < 1/2$ ($\lambda > 1/2$).

The asymptotic dynamics of this model qualitatively, and sometimes quantitatively, capture the phenomenology of the full problem. The model is fully tractable analytically and the detailed analysis is presented in App. E.2. We summarize here the main results:

- The left panels of Fig. 3 show the geometry of the problem in $1 + 1$ dimensions. It is easily seen that the optimal SVM solution is $s = 0, b = -1$ if and only if the data is not separable, i.e. when the segment $x_2 \geq 0$ contains the origin.
- The limiting value S_∞ can be easily found to be $S_\infty = \frac{1}{2(\lambda-1)} \log(1 - 2\lambda)$, for the separable case $\lambda < 1/2$. Indeed, it diverges logarithmically at $\lambda = 0.5$, in agreement with the numerical results of the full model presented in the upper-right panel of Fig. 1. The long time dynamics of $\|\mathbf{S}(t)\|$ and $b(t)$ are summarized in Table 1.
- The left panels of Fig. 4 show that the behavior of the loss and accuracy of the simplified model as a function of λ is remarkably similar to that of the full model.

	$\lambda < 0.5$ ($x_2 > 0$)	$\lambda = 0.5$ ($x_2 = 0$)	$\lambda > 0.5$ ($x_2 < 0$)
$b(t \gg 1)$	$-\log(t)$	$-\log(t)$	$-\frac{1}{1+M^2} \log(t)$
$\ \mathbf{S}\ (t \gg 1)$	$\frac{1}{2(1-\lambda)} \log\left(\frac{1}{1-2\lambda}\right)$	$\log(\log(t))$	$\frac{M}{1+M^2} \log(t)$

Table 1: Summary of the results in the different regimes in the simplified model, where $x_1 = -1$, $x_2 = 1 - 2\lambda$, and the margin is $M = |x_2| = 2\lambda - 1$.

4.1 Grokking Time and Universality

We begin by noting that the analytical result of $b(t)$ for $\lambda = 0.5$ can describe quite well the results of the full model, see middle panel of Fig. 1. This fact, combined with the assumption that the divergence of S_∞ of the full model is also logarithmic (as was verified numerically), the behavior of the Grokking time (defined below) is expected to be the same in both models. We will now calculate it in the simplified model.

We can define t_{tr}^* , t_{gen}^* as the times at which the training and generalization loss reach some threshold value ε . The singular part of these times can be calculated near criticality, as $\lambda \rightarrow \frac{1}{2}$ from below. The rigorous calculation is given in App. E.2 but the salient features can be obtained using simple scaling arguments:

Assume that σ is large enough such that the time it takes S to reach close to $S_\infty \approx \frac{1}{2} \log(1 - 2\lambda)$ is small. In this case, t_{tr}^* , t_{gen}^* are dominated by the time it takes b to diverge. Replacing S by S_∞ in the training loss, we find approximately $\mathcal{L}_{\text{tr}} \approx \frac{1}{2} e^b$. Using the asymptotic solution $b \approx -\log(\frac{\eta}{2}t)$, we immediately find $t_{\text{tr}}^* = \frac{1}{\eta\varepsilon}$. Similarly, the generalization loss takes the form $\mathcal{L}_{\text{gen}} = \mathbb{E}_{x \sim \mathcal{N}(0, \sigma)} [e^{Sx+b}] = e^{b + \frac{1}{2}\sigma^2 S^2}$, implying $t_{\text{gen}}^* = \frac{2}{\eta\varepsilon} e^{\frac{1}{2} \log^2(1-2\lambda)}$. It is already clear that for any finite ε , $\Delta t^* \equiv t_{\text{gen}}^* - t_{\text{tr}}^*$ diverges. We define an ε -independent quantity,

$$\frac{\Delta t^*}{t_{\text{tr}}^*} = e^{\frac{1}{2} \log^2(1-2\lambda)} - 1, \quad 0 < \lambda \leq 1/2, \quad (16)$$

which is verified numerically in Fig. 4. Further details can be found in App. E.3.

We note that this result bears a striking resemblance to that of [Levi et al., 2023], which employed the MSE loss in a linear regression problem, again for N points sampled iid from an isotropic Gaussian distribution. In their setting, the interpolation threshold is at $\lambda = 1$, in the sense that for $\lambda < 1$ the model always generalizes asymptotically, and never generalizes for $\lambda > 1$. They also found that the grokking time diverges logarithmically as a function of the distance from criticality, $(t_{\text{gen}}^* - t_{\text{tr}}^*)/t_{\text{tr}}^* \propto |\log(1 - \sqrt{\lambda})|$, which was explained in terms of a ‘‘critical slowing down’’ effect, arising from a vanishing eigenvalue of the data covariance near criticality. While the two problems are quite different, they both display a critical behavior near an effective interpolation threshold of the corresponding problem. We believe this is not a coincidence but rather a manifestation of a deeper relation between divergent behaviors in NNs and the intrinsic structure of the training data. We explore the various aspects of these universal properties in future work.

5 Conclusions and Limitations

In this work, we attempted to fill a gap in the Grokking literature, by sharply defining and tracking both empirically and analytically the ‘‘memorizing’’ and ‘‘generalizing’’ solutions in an interesting setting. We achieved this by constructing a simple yet informative example of ‘‘noise’’ classification, where the optimal solutions can always be found analytically.

Our work can be divided into two parts. First, we studied empirically the dynamics of ‘‘noise’’ classification, and demonstrated that grokking is clearly exhibited when the classifier transitions from the ‘‘memorizing’’ solution to the ‘‘generalizing’’ one. Additionally, we show that this grokking transition strongly depends on the underlying properties of the data, as it only occurs when the data is on the verge of being linearly separable from the origin in d dimensions, given by λ_c .

In the second part we presented a simple, one dimensional effective description of the full problem, and showed that it captures the salient properties leading to grokking. Employing this simple model, we are able to show that the grokking time diverges as the data becomes closer to linearly separable in d dimensions, and provide analytical predictions for the grokking time as a function of the properties of the data alone.

Finally, the existence of λ_c , which can be identified as the effective interpolation threshold for this problem, is a strong hint at the connection between grokking, and other emergent phenomena in deep learning, such as double descent. We will further address this connection in future work.

Limitations: We considered a specific problem of classifying irrelevant features, under a particular choice of feature distribution, namely, Normal with zero mean in high dimensions. It is natural to ask

how our results extend to more complex data, for instance including non-trivial correlations, hierarchical structure, or even a finite distribution (for instance [Gromov, 2023]). While we believe the same analysis can be repeated in these instances, in the sense of (non)linear separability, we leave this to future work.

All of the analytics were done in the GF limit, and while our results were verified by experiments with finite learning rate, it may be interesting to study how large learning rates effect this setup, possibly relating to catapults [Lewkowycz et al., 2020] or the edge of stability literature [Cohen et al., 2022].

Lastly, we did not study the prospect of nonlinear logistic regression, which is closer to deep learning models in the wild. We believe some of our results may be generalized, provided we accept a “feature map” description of the network up to the last layer, and consider the SVM solution on the learned features.

6 Acknowledgements

We thank Hillel Aharoni, Amit Moscovich and Daniel Soudry for fruitful discussions. YBS was supported by research grant ISF 1907/22 and Google Gift grant. NL is supported by the EPFL AI4science program.

Bibliography

- R. Anil, A. M. Dai, O. Firat, M. Johnson, D. Lepikhin, A. Passos, S. Shakeri, E. Taropa, P. Bailey, Z. Chen, et al. Palm 2 technical report. *arXiv preprint arXiv:2305.10403*, 2023.
- T. Brown, B. Mann, N. Ryder, M. Subbiah, J. D. Kaplan, P. Dhariwal, A. Neelakantan, P. Shyam, G. Sastry, A. Askell, et al. Language models are few-shot learners. *Advances in neural information processing systems*, 33:1877–1901, 2020.
- A. Chowdhery, S. Narang, J. Devlin, M. Bosma, G. Mishra, A. Roberts, P. Barham, H. W. Chung, C. Sutton, S. Gehrmann, et al. Palm: Scaling language modeling with pathways. *arXiv preprint arXiv:2204.02311*, 2022.
- B. Chughtai, L. Chan, and N. Nanda. A toy model of universality: Reverse engineering how networks learn group operations, 2023.
- J. M. Cohen, S. Kaur, Y. Li, J. Z. Kolter, and A. Talwalkar. Gradient descent on neural networks typically occurs at the edge of stability, 2022.
- T. M. Cover. Geometrical and statistical properties of systems of linear inequalities with applications in pattern recognition. *IEEE Transactions on Electronic Computers*, EC-14(3):326–334, 1965. doi: 10.1109/PGEC.1965.264137.
- X. Davies, L. Langosco, and D. Krueger. Unifying grokking and double descent. *arXiv preprint, arXiv:2303.06173*, 2023.
- D. Doshi, A. Das, T. He, and A. Gromov. To grok or not to grok: Disentangling generalization and memorization on corrupted algorithmic datasets, 2024.
- Google. Bard. 2023.
- A. Gromov. Grokking modular arithmetic. *arXiv preprint, arXiv:2303.02679*, 2023.
- A. H. Guth. Inflationary universe: A possible solution to the horizon and flatness problems. *Phys. Rev. D*, 23:347–356, Jan 1981. doi: 10.1103/PhysRevD.23.347. URL <https://link.aps.org/doi/10.1103/PhysRevD.23.347>.
- Z. Ji and M. Telgarsky. The implicit bias of gradient descent on nonseparable data. In *Conference on learning theory*, pages 1772–1798. PMLR, 2019.

- J. Kaplan, S. McCandlish, T. Henighan, T. B. Brown, B. Chess, R. Child, S. Gray, A. Radford, J. Wu, and D. Amodei. Scaling laws for neural language models, 2020.
- D. P. Kingma and J. Ba. Adam: A method for stochastic optimization, 2017.
- T. Kumar, B. Bordelon, S. J. Gershman, and C. Pehlevan. Grokking as the transition from lazy to rich training dynamics, 2023.
- N. Levi, A. Beck, and Y. Bar-Sinai. Grokking in linear estimators – a solvable model that groks without understanding, 2023.
- A. Lewkowycz, Y. Bahri, E. Dyer, J. Sohl-Dickstein, and G. Gur-Ari. The large learning rate phase of deep learning: the catapult mechanism, 2020.
- Z. Liu, O. Kitouni, N. S. Nolte, E. Michaud, M. Tegmark, and M. Williams. Towards understanding grokking: An effective theory of representation learning. *Advances in Neural Information Processing Systems*, 35:34651–34663, 2022.
- Z. Liu, E. J. Michaud, and M. Tegmark. Omnigrok: Grokking beyond algorithmic data, 2023.
- K. Lyu, J. Jin, Z. Li, S. S. Du, J. D. Lee, and W. Hu. Dichotomy of early and late phase implicit biases can provably induce grokking, 2024.
- W. Merrill, N. Tsilivis, and A. Shukla. A tale of two circuits: Grokking as competition of sparse and dense subnetworks, 2023.
- M. S. Nacson, J. D. Lee, S. Gunasekar, P. H. P. Savarese, N. Srebro, and D. Soudry. Convergence of gradient descent on separable data, 2019.
- N. Nanda, L. Chan, T. Liberum, J. Smith, and J. Steinhardt. Progress measures for grokking via mechanistic interpretability. *arXiv preprint arXiv:2301.05217*, 2023.
- P. J. T. Notsawo, H. Zhou, M. Pezeshki, I. Rish, and G. Dumas. Predicting grokking long before it happens: A look into the loss landscape of models which grok, 2023.
- OpenAI. Gpt-4 technical report. 2023.
- A. Power, Y. Burda, H. Edwards, I. Babuschkin, and V. Misra. Grokking: Generalization beyond overfitting on small algorithmic datasets. *arXiv preprint arXiv:2201.02177*, 2022.
- L. Prechelt. Early stopping-but when? In *Neural Networks*, 1996. URL <https://api.semanticscholar.org/CorpusID:14049040>.
- N. Rubin, I. Seroussi, and Z. Ringel. Grokking as a first order phase transition in two layer networks, 2024.
- R. Schaeffer, M. Khona, Z. Robertson, A. Boopathy, K. Pistunova, J. W. Rocks, I. R. Fiete, and O. Koyejo. Double descent demystified: Identifying, interpreting & ablating the sources of a deep learning puzzle, 2023.
- D. Soudry, E. Hoffer, M. S. Nacson, S. Gunasekar, and N. Srebro. The implicit bias of gradient descent on separable data. *Journal of Machine Learning Research*, 19(70):1–57, 2018. URL <http://jmlr.org/papers/v19/18-188.html>.
- S. Srivastava and G. Sharma. Omnivec: Learning robust representations with cross modal sharing, 2023.
- V. Thilak, E. Littwin, S. Zhai, O. Saremi, R. Paiss, and J. Susskind. The slingshot mechanism: An empirical study of adaptive optimizers and the grokking phenomenon. *arXiv preprint arXiv:2206.04817*, 2022.

- A. Vaswani, N. Shazeer, N. Parmar, J. Uszkoreit, L. Jones, A. N. Gomez, L. Kaiser, and I. Polosukhin. Attention is all you need, 2023.
- J. Wendel. A problem in geometric probability. *Mathematica Scandinavica*, 11:109–112, 1962. URL <http://eudml.org/doc/165817>.
- Z. Xu, Y. Wang, S. Frei, G. Vardi, and W. Hu. Benign overfitting and grokking in relu networks for xor cluster data, 2023.
- A. Zeng, X. Liu, Z. Du, Z. Wang, H. Lai, M. Ding, Z. Yang, Y. Xu, W. Zheng, X. Xia, et al. Glm-130b: An open bilingual pre-trained model. *arXiv preprint arXiv:2210.02414*, 2022.
- B. Žunkovič and E. Ilievski. Grokking phase transitions in learning local rules with gradient descent, 2022.

Appendix

A Separability and Wendel’s Theorem

Wendel’s theorem [Wendel, 1962] states that the probability that N random vectors drawn from an isotropic distribution in d dimensions is

$$p = \frac{1}{2^{N-1}} \sum_{k=0}^{d-1} \binom{N-1}{k} \quad (17)$$

This is the cumulative probability function of the Binomial distribution, i.e. the probability that the number of successes is greater than d out of $N-1$ attempts with success probability $\frac{1}{2}$. The central limit theorem states that in the limit of large N, d the binomial distribution approaches a Gaussian, and thus the cumulative distribution function approaches the error function. Straightforward algebra gives that for large N, d we have

$$p(\lambda) \rightarrow \frac{1}{2} \left[1 + \operatorname{erf} \left(\sqrt{d} \left(\sqrt{2\lambda} - \frac{1}{\sqrt{2\lambda}} \right) \right) \right], \quad \lambda = \frac{d}{N}. \quad (18)$$

It is seen that for $d \rightarrow \infty$ the transition becomes infinitely sharp as a function of lambda and we have

$$\lim_{d \rightarrow \infty} p(\lambda) = \begin{cases} 0 & \lambda < \frac{1}{2} \\ \frac{1}{2} & \lambda = \frac{1}{2} \\ 1 & \lambda > \frac{1}{2} \end{cases} \quad (19)$$

See also Cover [1965] for further discussion.

B Relation to canonical examples

In this section, we will discuss the similarities and differences of our work with previous examples of Grokking in the literature, focusing on the seminal work of Power et. al. [Power et al., 2022]. We first note that Grokking at Power et. al. is significant when the fraction of the data used for training $\alpha = N_{\text{training}}/N$ is near a critical value α_c , in the sense that the system achieves perfect generalization if and only if $\alpha > \alpha_c$, as can be seen in Fig. 1 (center) of their paper. We expect that this non-analytic behavior in the long time limit of training will be the crucial property that underlies grokking. That is, we expect that near such points the dynamics will be slow. We note that α in Power et. al. is analogous to our λ parameter, defining an effective "interpolation threshold" for the modular arithmetic problem.

Secondly, we note that a noticeable difference between our work and that of Power et. al. is that in our case, the accuracy shows a rise from the start rather than staying at chance level for a long time before generalizing. We argue that this is only a superficial discrepancy that depends on the choice of optimizer and fine-tuning of hyperparameters, and that the fundamental mechanism (that grokking occurs near critical points in which solutions exchange stability and dynamics are generically slow) is the same.

Indeed, in Fig. 5 we show that our setup is capable of grokking with accuracy staying at chance level (50%) at the start, similar to Power et al. We achieved this by using λ values closer to half ("almost separable") and the Adam optimizer instead of vanilla gradient descent (GD). The fact that this optimizer converges faster on the training data is no coincidence: the adaptive learning rate leads to quicker convergence to large values of $|S|$ (the "memorizing solution"), maintaining accuracy at chance level until later stages, before going to large $-b$ (the "generalizing solution"). Notably, Power et al. also used Adam (or AdamW). In conclusion, although Adam can lead to a slightly "cleaner" grokking result, we explored GD because it is easier to derive analytical insights from it while, we believe, not changing the underlying mechanism of grokking. Finally, We will also note that the non-monotonicity of the test loss is also a typical sign of Grokking that can be seen in our setup (for example, compare Fig. 4 of Power et al. with the test loss in Fig. 5).

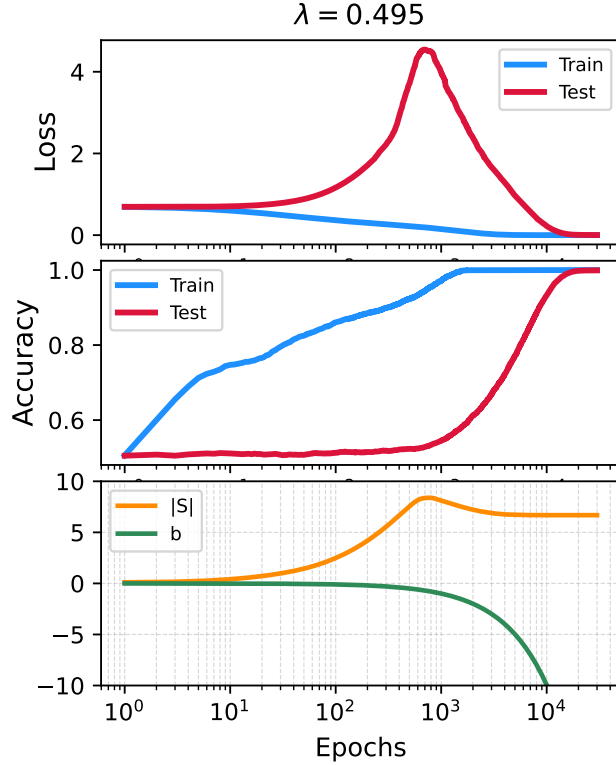


Figure 5: Grokking in a similar setup to the results in the main text but with ADAM optimizer (with $\beta_1 = 0.8$, $\beta_2 = 0.9$), instead of GD. The parameters are $\lambda = d/N = 0.495$, $N = 4000$ and $\sigma = 1$.

C Divergence of the conformal time

In the main text we have defined the “conformal time” $\tau = \int_0^t e^{b(t')} dt'$ and saw that as the result the gradient-descent trajectory of $\mathbf{S}(t)$ is the same as one that minimizes the exponential loss without bias: $\mathcal{L} = \frac{1}{N} \sum_{i=1}^N e^{\mathbf{S}^T \mathbf{x}_i}$. However, if τ is bounded it might reach a different fixed point. We will show now that indeed τ must diverge. First, we notice that the loss must be bounded from above: If the points are not separable (that is, there is some $\varepsilon > 0$ such that for any $\frac{\mathbf{S}^T}{\|\mathbf{S}\|}$ that we choose $\frac{\mathbf{S}^T}{\|\mathbf{S}\|} \mathbf{x}_i > \varepsilon$ for any i), then it must be true since $\|\mathbf{S}\|$ is bounded — otherwise the loss would be infinite. If the points are separable, then $\|\mathbf{S}\|$ might diverge (and will, as discussed in the main text) but at some point all of the arguments of the exponent would be negative, so the loss would be trivially bounded by 1. Now, using the fact that $\frac{\partial \beta}{\partial t} = \beta \frac{\partial b}{\partial t}$ we have $\frac{\partial \beta}{\partial t} = -\eta \beta^2 \frac{1}{N} \sum_i e^{\mathbf{S}^T \mathbf{x}_i}$. Denoting $\mathcal{L}(t) < C$, we see that

$$-\frac{1}{\beta^2} \frac{\partial \beta}{\partial t} < \eta C. \quad (20)$$

We note that on the left-hand side we have a positive function (since $\frac{\partial \beta}{\partial t} < 0$). In other words, $\frac{\partial}{\partial t} \left[\frac{1}{\beta(t)} \right] < \eta C$, so we get that

$$\frac{1}{\beta(t)} = \frac{1}{\beta(0)} + \int_0^t \frac{\partial}{\partial t} \left[\frac{1}{\beta(t)} \right] < \frac{1}{\beta(0)} + \int_0^t \eta C = \frac{1}{\beta(0)} + \eta C t \quad (21)$$

so that $\frac{1}{\beta(t)} < 1 + \eta C t$ or, $\beta(t) > \frac{1}{1 + \eta C t}$. This means that $\int_0^t \beta(t) > \int_0^t \frac{1}{1 + \eta C t}$, which diverges.

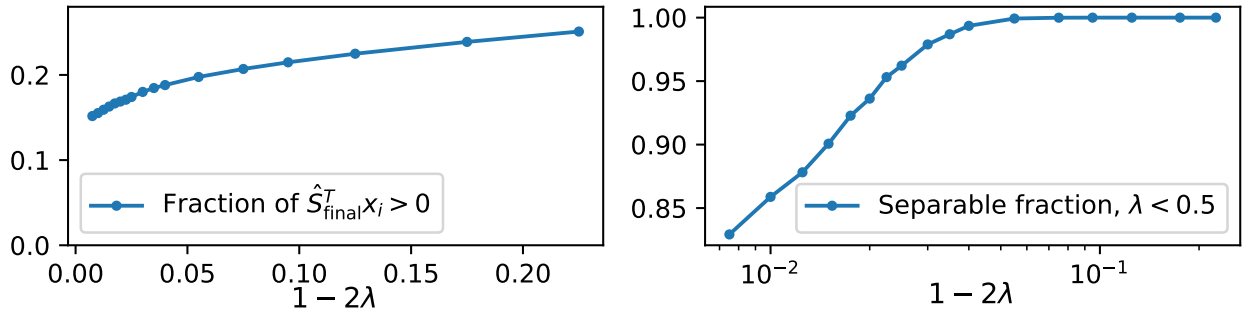


Figure 6: Left panel: The fraction of positive $\frac{\mathbf{S}_{\infty}^T}{\|\mathbf{S}_{\infty}\|} \mathbf{x}_i$, which goes to a constant for $\lambda = 0.5$. Right panel: The fraction of separable datasets for $\lambda < 0.5$ that were not included in the calculation.

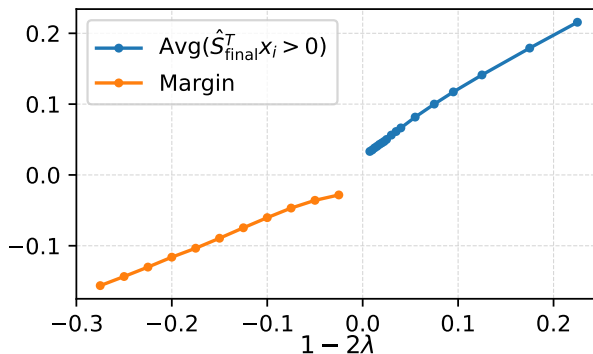


Figure 7: Numerical investigation of properties of the limiting distribution of $\mathbf{S}^T \mathbf{x}_i$, as a function of $1 - 2\lambda$ (averaged over different random configurations). In blue, we plot the average value of positive $\frac{\mathbf{S}_{\infty}^T}{\|\mathbf{S}_{\infty}\|} \mathbf{x}_i$, for $\lambda < 0.5$ (by minimizing $\mathcal{L} = \frac{1}{N} \sum_{i=1}^N e^{\mathbf{S}^T \mathbf{x}_i}$), and the margin for $\lambda > 0.5$ (using SVM).

D Proof that S_{∞} diverges for almost separable data

We look at the function

$$f(S, \{x_i\}) = \sum_{i=1}^n e^{\mathbf{S} \cdot x_i} \quad x, S \in \mathbb{R}^d \quad (22)$$

We will assume $n > d$ and that the data is in general position, and that it is not separable from the origin. Since for every S we must have $S \cdot x_i > 0$ for some i , it is easy to see that f diverges when S grows large in any direction. Since $f > 0$, there exists a global minimum at finite S .

A minimum (which is also unique under our assumptions but that's not crucial) obeys

$$\frac{\partial f}{\partial S} = \sum_{i=1}^n x_i e^{\mathbf{S} \cdot x_i} = 0 \quad (23)$$

If we divide this expression by f , we get

$$\sum_{i=1}^n p_i x_i = 0 \quad p_i = \frac{e^{\mathbf{S} \cdot x_i}}{f} \quad 0 \leq p_i \leq 1, \quad \sum_i p_i = 1 \quad (24)$$

Eq. (24) means that the origin is a convex combination of the sample points with weights p_i . We found that a necessary condition for the existence of a critical point at a finite S is that the origin is contained in the convex hull of the sample points. This is of course equivalent to the condition that the origin is not linearly separable from the sample data.

We want to show that if the data is almost separable, that is, if it is not separable but the origin

is close to the boundary of the convex hull, then S must be large. The intuition for this comes from Eq. (24): if the origin is very close to the boundary of the convex hull then some of the p_i 's must be very large compared to the others, which can only happen if S is large.

In fact, the origin is *exactly* on the boundary of the convex hull (that is, the data is exactly on the edge of separability) if and only if for every representation of the origin as a convex combination of the sample points,

$$\sum_{i=1}^n q_i x_i = 0, \quad (25)$$

the weights q_i are non zero only for k sample points, say x_i, \dots, x_k , with $k \leq d$, and x_1, \dots, x_k are the vertices of a facet of the convex hull. This naturally leads to the definition:

Definition We say that the origin is ϵ -close to the boundary if there exist k points x_1, \dots, x_k such that for every representation of the type of Eq. (25), the total weight assigned to x_1, \dots, x_k is at least $1 - \epsilon$,

$$\sum_{i=1}^k q_i \geq 1 - \epsilon$$

Theorem If the origin is ϵ -close to the boundary of the convex hull of the sample points, then the norm of $S = \operatorname{argmin} f$ is bounded from below by

$$|S| \geq \frac{1}{D} \log \left(\frac{1 - \epsilon}{\epsilon} \right)$$

where $D = \max_{i,j} |x_i - x_j|$ is the diameter of the data.

Proof. We divide the points to two groups: $A = \{x_1, \dots, x_k\}$, and $B = \{x_{k+1}, \dots, x_N\}$. Since the origin is ϵ -close, the ratio of the weights of the two groups is bounded by

$$\frac{\sum_{i \in A} p_i}{\sum_{i \in B} p_i} \geq \frac{1 - \epsilon}{\epsilon} \quad (26)$$

Consider now the convex combination Eq. (24). Using Jensen's inequality, we can bound the relative weights of the second group by

$$\sum_{i \in B} e^{S \cdot x_i} \geq (N - k) e^{S \cdot \bar{x}}, \quad \text{with} \quad \bar{x} = \frac{1}{N - k} \sum_{i \in B} x_i \quad (27)$$

where \bar{x} is the average of the points in the second group. Therefore, the ratio is bounded by

$$\frac{\sum_{i \in A} p_i}{\sum_{i \in B} p_i} = \frac{\sum_{i \in A} e^{S \cdot x_i}}{\sum_{i \in B} e^{S \cdot x_i}} \leq \frac{\sum_{i \in A} e^{S \cdot x_i}}{(N - k) e^{S \cdot \bar{x}}} \leq \frac{k}{N - k} e^{|S|D} \leq \frac{k}{N - k} e^{|S|D} \quad (28)$$

Combining Eq. (26) and Eq. (28) we get

$$\frac{1 - \epsilon}{\epsilon} \leq \frac{k}{N - k} e^{|S|D} \quad \Rightarrow \quad |S| \geq \frac{1}{D} \log \left(\frac{1 - \epsilon}{\epsilon} \cdot \frac{N - k}{k} \right) \quad (29)$$

Since $k \leq d$, we also have $N - k \geq n - d$.

Note that the same convexity argument would work also for logistic loss $f = \sum_i \ell(S \cdot x_i)$, $\ell(z) = \log(1 + e^z)$, or any other monotonic and convex ℓ . In this case the only difference is that the log function should be replaced the inverse of ℓ . \square

E Details of the Simplified Model

E.1 Justification and Relation to the Full Model

We will provide here supplemental results regarding the justification of the simplified model (by numerical comparison to the full model). To obtain the results we average over different random

realizations: Assuming the so-called ‘‘self averaging’’ property, we know that the average over a large number of finite systems should give us the same result as the infinite system (where $N, d \rightarrow \infty$ and the ratio is constant).

In the non-separable case, \mathbf{S}_∞ can be found by any optimizer that minimizes the loss $\mathcal{L} = \sum e^{\mathbf{S}^T \mathbf{x}_i}$. We note that when getting close to the transition point, for any finite-sized system we have some probability of getting a separable set (even though $\lambda < 0.5$), see Eq. (17). In this case, we just ignore the the result: In the right panel of Fig. 6 we present the fraction of realizations that are separable. This will probably introduce some bias into the results which is likely the cause of the fact that the average of positive samples (and similarly, the margin) does not go exactly to zero for $\lambda \rightarrow 0.5$ (see Fig. 7). In the left panel of Fig. 6 we present the fraction of positive $\frac{\mathbf{S}_\infty^T}{\|\mathbf{S}_\infty\|} \mathbf{x}_i$. Interestingly, it does not go to zero but to some positive constant, implying that there is a singularity in the density of $\frac{\mathbf{S}_\infty^T}{\|\mathbf{S}_\infty\|} \mathbf{x}_i$ at $\lambda = 0.5$.

E.2 Analytical Predictions

Here, we provide the full analysis of the model presented in Sec. 4, for a single point fixed at $x_1 = -1$, and a second point $x_2 = x = 1 - 2\lambda$, where $\lambda = d/N$.

The gradient flow equations in conformal time are given by

$$\begin{aligned} \frac{\partial S}{\partial \tau} &= -\frac{\eta}{2} (xe^{Sx} - e^{-S}) = -\frac{\eta}{2} \left((1 - 2\lambda)e^{S(1-2\lambda)} - e^{-S} \right), \\ \frac{\partial b}{\partial \tau} &= -\frac{\eta}{2} (e^{Sx} + e^{-S}) = -\frac{\eta}{2} \left(e^{S(1-2\lambda)} + e^{-S} \right). \end{aligned} \quad (30)$$

While there exist analytical solutions for Eq. (30), they do not necessarily provide any intuition, and so we find it better to begin by investigating three special representative cases:

1. $x_2 = 1$ (non-separable).
2. $x_2 = 0$ (marginally non-separable).
3. $x_2 = -1$ (separable).

For $x = 1$ (A), the data is entirely non-separable in one dimension and the conformal time solutions are

$$\begin{aligned} S(\tau) &= \log \left(\tanh \left(\frac{\eta\tau}{2} + \tanh^{-1} (e^{S_0}) \right) \right), \\ b(\tau) &= b_0 + \log \left(\frac{\tanh (2 \tanh^{-1} (e^{S_0})) \cosh (2 \tanh^{-1} (e^{S_0}))}{\tanh (\eta\tau + 2 \tanh^{-1} (e^{S_0})) \cosh (\eta\tau + 2 \tanh^{-1} (e^{S_0}))} \right), \end{aligned} \quad (31)$$

in which case the generalization accuracy reaches 1 for $\tau \rightarrow \infty$, as $b(\tau)$ grows faster than $S(\tau)$ with conformal time.

For $x_2 = 0$ (B), the equations in conformal time become:

$$\frac{\partial S}{\partial \tau} = \frac{\eta}{2} e^{-S}, \quad \frac{\partial b}{\partial \tau} = -\frac{\eta}{2} (e^{-S} + 1) \quad (32)$$

By solving for S and plugging into $\frac{\partial b}{\partial \tau}$, we immediately get

$$S = \log \left(e^{S_0} + \frac{\eta}{2} \tau \right), \quad b = -\log \left(e^{S_0} + \frac{\eta}{2} \tau \right) - \frac{\eta}{2} \tau + S_0 + b_0. \quad (33)$$

Using the fact that $e^b = \frac{\partial \tau}{\partial t}$, we get that $\frac{\partial \tau}{\partial t} = \frac{e^{-\frac{\eta}{2}\tau}}{e^{S_0 + \frac{\eta}{2}\tau}} e^{S_0 + b_0}$, and taking another integral, we get that $e^{\frac{\eta}{2}\tau} [e^{S_0} - 1 + \frac{\eta}{2}\tau] = e^{S_0 + b_0} \frac{\eta}{2} t + (e^{S_0} - 1)$. Taking the inverse of this, we finally get

$$\tau = \frac{2}{\eta} \left[W_0 \left(\left(e^{S_0 + b_0} \frac{\eta}{2} t + (e^{S_0} - 1) \right) e^{e^{S_0} - 1} \right) - e^{S_0} + 1 \right], \quad (34)$$

where W_0 is the Lambert W function. We note that for large t we have $\tau \sim \log(t)$, and therefore $b \sim -\log(t)$, $S \sim \log(\log(t))$, so it is interesting to note that in the critical point we still have $\lim_{t \rightarrow \infty} S(t)/b(t) = 0$ (i.e., accuracy goes to 1), even though S diverges.

Finally, for $x = -1$ (C), the data is fully separable in one dimension and the solution in conformal time is given by

$$S(\tau) = S_0 + \log(1 + \eta\tau e^{-S_0}), \quad b(\tau) = b_0 - \log(1 + \eta\tau e^{-S_0}), \quad (35)$$

showing that the accuracy is bounded at $\mathcal{A}_{\text{gen}}^\infty = \frac{1}{2} \left(1 + \operatorname{erf}\left(\frac{1}{\sqrt{2}}\right)\right)$ agreeing with the results of Eq. (13) where $M = 1$.

For completeness, we report here the full solution, as a function of the conformal time $\tau = \int_0^t e^{b(t)} dt$ of Eq. (30). We define

$$f(y) = -\frac{x e^{y(x+2)} {}_2F_1\left(1, 1 + \frac{1}{x+1}; 2 + \frac{1}{x+1}; e^{(x+1)y} x\right)}{x+2} - e^y, \quad (36)$$

then the solution for $S(\tau)$ is given by the inverse function $f^{-1}(u)$ evaluated at

$$u = -\frac{x e^{S_0(x+2)} {}_2F_1\left(1, 1 + \frac{1}{x+1}; 2 + \frac{1}{x+1}; e^{S_0(x+1)} x\right)}{x+2} - \frac{\tau}{2} - e^{S_0}, \quad (37)$$

as

$$S(\tau) = f^{-1}\left(-\frac{x e^{S_0(x+2)} {}_2F_1\left(1, 1 + \frac{1}{x+1}; 2 + \frac{1}{x+1}; e^{S_0(x+1)} x\right)}{x+2} - \frac{\eta\tau}{2} - e^{S_0}\right). \quad (38)$$

The solution for $b(\tau)$ is obtained simply by integrating Eq. (30), resulting in

$$\begin{aligned} b(\tau) = \frac{1}{x} & \left[b_0 x - \log\left(1 - e^{(1+x)f^{-1}\left(-e^{S_0} - \frac{e^{S_0(2+x)} x {}_2F_1\left(1, 1 + \frac{1}{x+1}; 2 + \frac{1}{x+1}; e^{S_0(1+x)} x\right)}{2+x}\right)}\right) x \right] \\ & + \log\left(1 - e^{(1+x)f^{-1}\left(-e^{S_0} - \frac{\eta\tau}{2} - \frac{e^{S_0(2+x)} x {}_2F_1\left(1, 1 + \frac{1}{x+1}; 2 + \frac{1}{x+1}; e^{S_0(1+x)} x\right)}{2+x}\right)}\right) x \\ & + x f^{-1}\left(-e^{S_0} - \frac{e^{S_0(2+x)} x {}_2F_1\left(1, 1 + \frac{1}{x+1}; 2 + \frac{1}{x+1}; e^{S_0(1+x)} x\right)}{2+x}\right) \\ & - x f^{-1}\left(-e^{S_0} - \frac{\eta\tau}{2} - \frac{e^{S_0(2+x)} x {}_2F_1\left(1, 1 + \frac{1}{x+1}; 2 + \frac{1}{x+1}; e^{S_0(1+x)} x\right)}{2+x}\right) \right]. \end{aligned} \quad (39)$$

While these solutions may not necessarily be instructive in this form, appropriate limits can be taken in order to obtain the results in the main text.

E.3 Grokking time in the simplified model

We can define t_{tr}^* , t_{gen}^* as the times it would take for the training and generalization loss to reach some threshold ε . We can find t_{tr}^* by solving $\mathcal{L}_{\text{tr}} = \frac{1}{2} e^b (e^{-S} + e^{S(1-2\lambda)}) = \varepsilon$. We will assume that σ is large enough such that $S = S_\infty$ from the start (as discussed in the main text, σ increase the rate that S goes to its final value). Therefore, we plug $S_\infty = -\log(1 - 2\lambda)$, and find that for λ which is close enough to 0.5, the loss is approximately given by $\mathcal{L}_{\text{tr}} = \frac{1}{2} e^b$. Comparing to ε and plugging the long-time limit $b = -\log(\frac{\eta}{2}t)$, we find that

$$t_{\text{tr}}^* = \frac{1}{\eta\varepsilon}. \quad (40)$$

Similarly, using the generalization loss $\mathcal{L}_{\text{gen}} = e^b e^{S^2/2}$ we can find that

$$t_{\text{gen}}^* = \frac{2}{\eta\varepsilon} e^{\frac{1}{2} \log^2(1-2\lambda)} \quad (41)$$

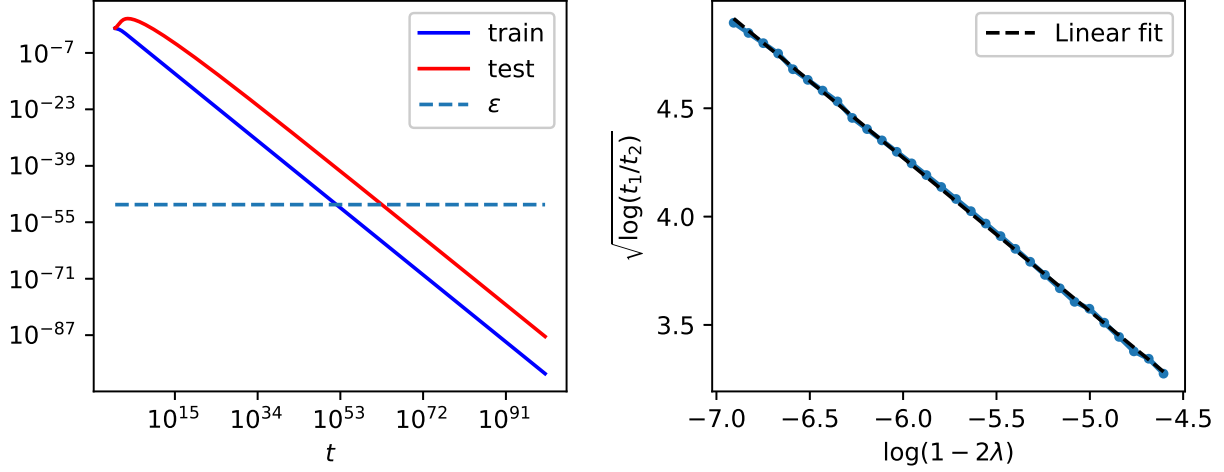


Figure 8: Numerical evidence for the Grokking time in the simplified model. In the left panel, we demonstrate for $1 - 2\lambda = 0.001$ how the Grokking time is calculated: t_{tr}^* , t_{gen}^* are calculated by finding the intersection of the loss with some ε . In the right panel we plot $\sqrt{\log(t_{\text{gen}}^*/t_{\text{tr}}^*)}$ versus $\log(1 - 2\lambda)$ numerically, and show that the result is linear with slope $\approx \frac{1}{\sqrt{2}}$, in agreement with the prediction of Eq. (42)

It is already clear that for any finite ε , $t_{\text{gen}}^* - t_{\text{tr}}^*$ diverges. We can also obtain an ε -independent property by noting that

$$\sqrt{\log(t_{\text{gen}}^*/t_{\text{tr}}^*)} = \frac{1}{\sqrt{2}} \log(1 - 2\lambda), \quad (42)$$

which is verified numerically in Fig. 8.

It is interesting to note that in the conformal time, we have $b \approx -\tau$, and therefore can repeat this calculation and obtain

$$\tau_{\text{tr}}^* = -\log(\eta\varepsilon), \quad \tau_{\text{gen}}^* = \frac{1}{2} \log^2(1 - 2\lambda) - \log \frac{\eta}{2} \varepsilon. \quad (43)$$

In this case, the result is a bit more natural since now the time difference (instead of ratio) becomes ε -independent:

$$\tau_{\text{gen}}^* - \tau_{\text{tr}}^* \approx \frac{1}{2} \log^2(1 - 2\lambda). \quad (44)$$

We note that this result still depends on ε implicitly, in the sense that our assumption that $S = S_\infty$ is true only for long-times, or ε which is small enough.

E.4 Calculation of the subleading term in the separable case

We now consider $x_2 < 0$ but close to zero (that is, we are in a separable case where $M = -x_2$ is the margin). We know that w diverges at long times as $w \approx \frac{M}{1+M^2} \log \left[\frac{\eta}{2} (1 + M^2)t + 1 \right]$. We will now denote

$$u \equiv w - \frac{M}{1 + M^2} \log \left[\frac{\eta}{2} (1 + M^2)t + 1 \right]$$

as the difference from the diverging term. The equation for u is therefore

$$\frac{\partial u}{\partial t} = -\frac{\eta}{2} e^b \left(-e^{x_1 \left(u + \frac{M}{1+M^2} \log \left[\frac{\eta}{2} (1+M^2)t \right] \right)} - M e^{-M \left(u + \frac{M}{1+M^2} \log \left[\frac{\eta}{2} (1+M^2)t \right] \right)} \right) - \frac{M}{1 + M^2} \frac{1}{t}.$$

Plugging the (long-time) solution for the bias, $b \approx -\frac{1}{M^2+1} \log \left[\frac{\eta}{2}(1+M^2)t + e^{-(1+M^2)b_0} \right]$ (where $b_0 = 0$ in our case), we get

$$\frac{\partial u}{\partial t} = -x_1 \frac{\eta}{2} e^{x_1 u} \left(\frac{\eta}{2}(1+M^2)t + 1 \right)^{\frac{x_1 M - 1}{1+M^2}} + (e^{-Mu} - 1) \frac{M}{(1+M^2)t + \frac{2}{\eta}}.$$

For $M \approx 0$, we note that the second term is $O(M^2)$, and by neglecting it we get

$$u = -\frac{1}{x_1} \log \left(\frac{x_1^2}{x_1 M + M^2} \left(\frac{\eta}{2}(1+M^2)t + 1 \right)^{\frac{x_1 M + M^2}{1+M^2}} - \frac{x_1^2}{x_1 M + M^2} + 1 \right).$$

For $t \rightarrow \infty$, and neglecting the other $O(M^2)$ terms, we finally get

$$u \approx -\frac{1}{x_1} \log \left(\frac{x_1}{x_2} \right).$$

Remarkably, this is identical to the result of the in the $x_2 > 0$ case.

F Impact of different parameters

Here we present supplemental results for Sections 3.4.

F.1 The Variance Scale σ

Here we provide additional information regarding the effect of σ different than 1. In particular, we will show that increasing σ can make grokking more apparent (but only up to a certain point). We will first assume that $\sigma = 1$ at the start, and investigate how taking $\tilde{\mathbf{x}}_i = \sigma \mathbf{x}_i$ changes the dynamics in comparison to that case. We will begin with the non-separable case ($\lambda < 0.5$). Recalling that the equations for gradient flow in our model are given by Eq. (9), this results in

$$\frac{\partial \mathbf{S}}{\partial t} = -\sigma \frac{\eta}{N} e^b \sum_i e^{\mathbf{S}^T \sigma \mathbf{x}_i} \mathbf{x}_i, \quad \frac{\partial b}{\partial t} = -\frac{\eta}{N} e^b \sum_i e^{\mathbf{S}^T \sigma \mathbf{x}_i}. \quad (45)$$

We can now absorb σ into \mathbf{S} by denoting $\tilde{\mathbf{S}} \equiv \sigma \mathbf{S}$ and investigate how it affects the dynamics of $\tilde{\mathbf{S}}$, and the generalization loss and accuracy as a function of $\tilde{\mathbf{S}}$. First, the GD equations become

$$\frac{\partial \tilde{\mathbf{S}}}{\partial t} = -\sigma^2 \frac{\eta}{N} e^b \sum_i e^{\tilde{\mathbf{S}}^T \mathbf{x}_i} \mathbf{x}_i, \quad \frac{\partial b}{\partial t} = -\frac{\eta}{N} e^b \sum_i e^{\tilde{\mathbf{S}}^T \mathbf{x}_i}. \quad (46)$$

We note that the generalization loss and accuracy in Eqs. (5) and (6) are the same except they are now a function of $\|\tilde{\mathbf{S}}\|$ instead of $\|\mathbf{S}\|$ (being a function of $\sigma \|\mathbf{S}\|$). Since the equation for $\frac{\partial \tilde{\mathbf{S}}}{\partial t}$ is just multiplied by a factor σ^2 , the limiting value of $\tilde{\mathbf{S}}_\infty$ would be the same as for the $\sigma = 1$ case, but it will reach it at a *faster rate*. To sum up, obtaining the dynamics of the loss and accuracy when σ is larger than one can be done by using the same Eqs. (5) and (6), but also (A) Increasing the starting condition of \mathbf{S}_0 by a factor of σ , and (B) Multiply only the learning rate of the spatial part by a factor of σ^2 . If σ is large enough, we can go to the fixed point of $\|\mathbf{S}\|$ as fast as we want, enabling the appearance of Grokking (if also the limiting value of $\|\mathbf{S}\|$ is large, which happens when we are on the edge of being separable).

Finally, we will also investigate the effect of σ in the separable regime ($\lambda > 0.5$). Now we can use Eqs. (12) and (13), where we only need to consider how σ changes the margin M . Since it is obtained from the equation $\frac{\mathbf{S}^T}{\|\mathbf{S}\|} x_m = -M$, we can see that the new margin will be larger by σ than the old one, i.e., $\tilde{M} = \sigma M$. Plugging this in Eq. (13), we get that the accuracy is now

$$\lim_{t \rightarrow \infty} \mathcal{A}_{\text{gen}} \approx \frac{1}{2} \left[1 + \text{erf} \left(\frac{1}{\sigma^2 M \sqrt{2}} \right) \right]. \quad (47)$$

where we note that the argument inside the erf is smaller in a factor of σ^2 , drastically reducing the limiting accuracy.

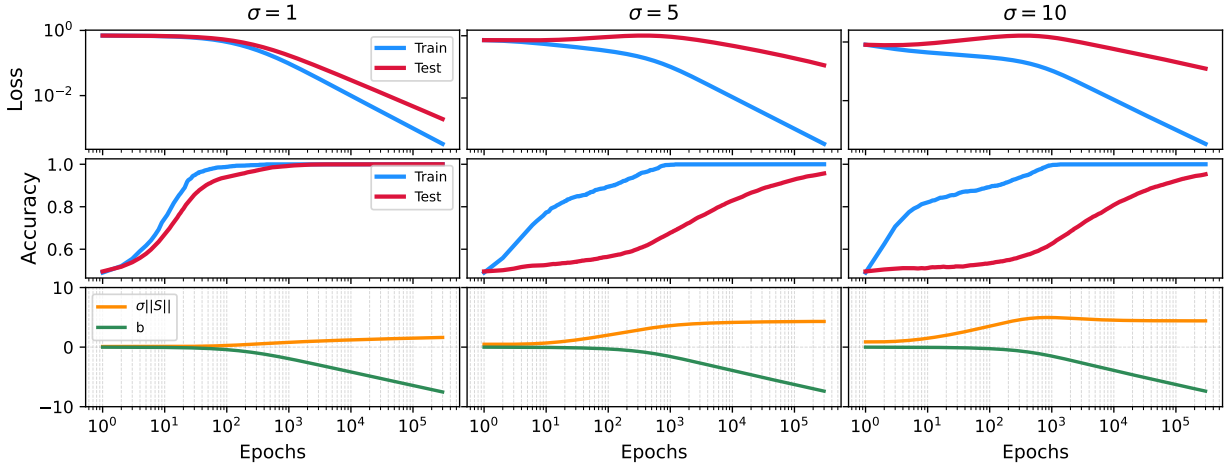


Figure 9: Gradient descent dynamics for three different values of σ , all for $\lambda = 0.48$. The top panels show the loss and accuracy for the train and test datasets, while the bottom panels present b and the norm of \mathbf{S} . Except for σ , the parameters are the same as in Fig. 1. We can see that increasing σ makes the grokking more apparent at start, but then saturates (that is, increasing σ will not increase the “grokking time” anymore).

F.2 Optimizer

The effect of changing the optimizer to Adam is demonstrated in Fig. 10. We note that the fact that adaptive-type optimizers change each learning rate individually based on past gradients, leads the dynamics faster in the direction of $\|\mathbf{S}\|$, relatively to b . The fact that it makes $\|\mathbf{S}\|$ change faster (and not slower) than b , is probably related to the fact that \mathbf{S} is a vector in high dimension: Moving each component of such vector will result in a change of the norm in a rate that is proportional to \sqrt{d} , but this may need further investigation. We will also note that using a different optimizer for the non-separable region where, will lead to a different solution than the hard margin SVM, as is also discussed by Soudry et al. [Soudry et al., 2018]. This means that the results we developed in the main text will not hold, but we can still expect to obtain accuracy smaller than one since $\|\mathbf{S}\|$ diverges, as indeed can be seen in Fig. 10.

F.3 Initial conditions

As discussed in the main text, changing the initial conditions can change the monotonicity of the generalization loss and accuracy: See Fig. 11, 12 below.

F.4 Different loss

In the main text, we showed that we can use the exponential instead of the CE loss, since it will converge to it at late times. Here we provide numerical evidence that indeed Grokking could be seen, even when taking from the beginning just the exponential loss $\mathcal{L} = \frac{1}{N} \sum_i e^{\mathbf{S}^T x_i + b}$: See Fig. 13.

G Direct calculation of the late time behavior of b, \mathbf{S} in the separable regime

Here we present a direct calculation for $\mathbf{S}(t) \equiv \|\mathbf{S}(t)\| \hat{\mathbf{S}}(t)$, $\mathbf{b}(t)$ at late times. First, we will work in the conformal time $\tau = \int_0^t \beta(t') dt'$. As discussed in the main text, when the data is separable we know that in the late time limit $\hat{\mathbf{S}}$ goes to a certain direction and $\|\mathbf{S}\| \rightarrow \infty$. Therefore, only the points

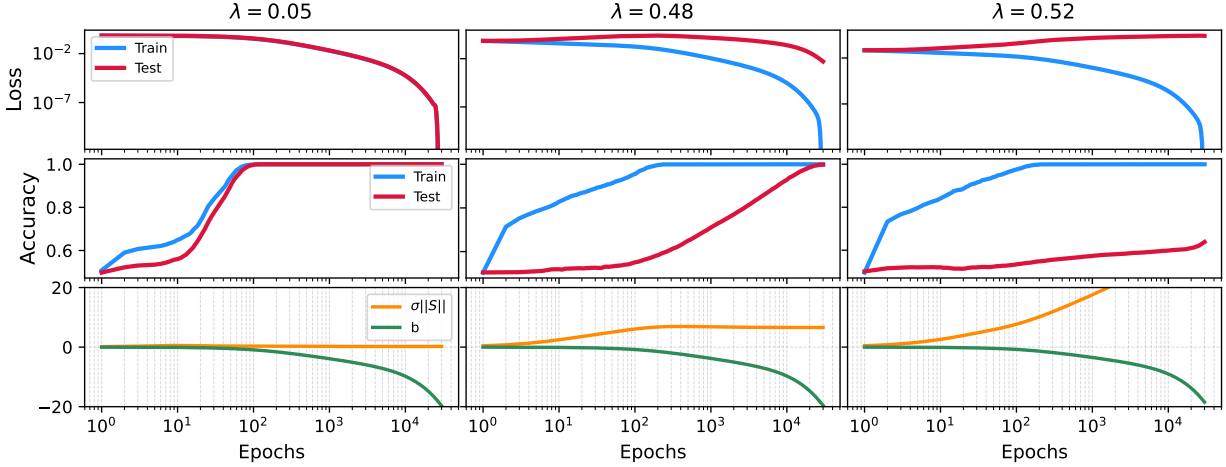


Figure 10: Dynamics, using ADAM optimizer with PyTorch’s default parameters. The setup is the same as Fig. 1, except for the fact that $\sigma = 1$ now instead of 5. Significant Grokking can be seen even though the value of σ is not large.

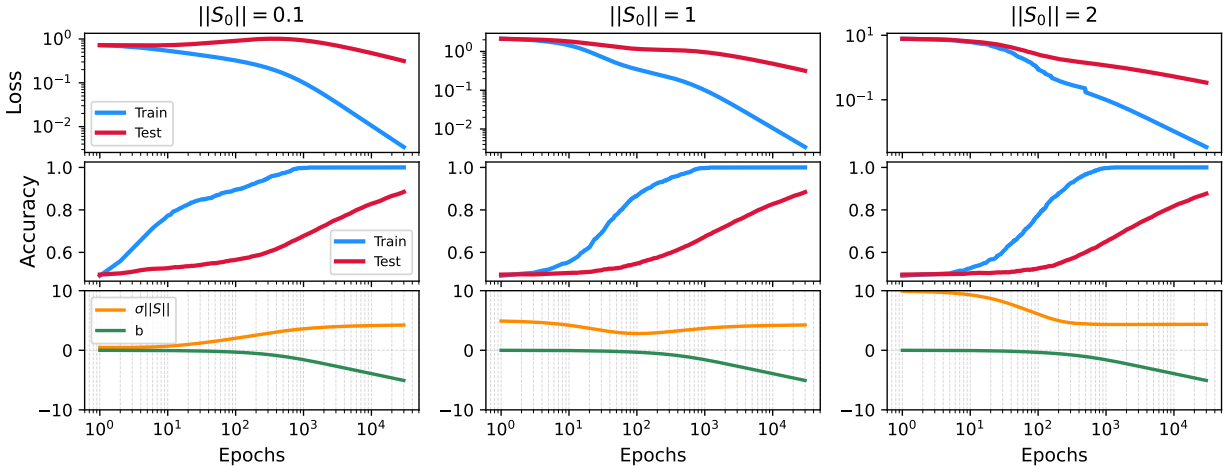


Figure 11: Gradient descent dynamics for $\lambda = 0.48$ and for three different values of starting norm, $\|\mathbf{S}_0\|$. Except for this, the setup is the same as Fig. 1. We can see that the non-monotonicity of the loss can be affected by the starting condition.

with maximum $\mathbf{S}^T x_m$ will contribute to the sum in the large

$$\frac{1}{N} \sum_i e^{\mathbf{S}^T x_i} \approx \frac{D}{N} e^{\mathbf{S}^T x_m}, \quad (48)$$

where $\mathbf{S}^T x_m$ is the maximum value that is obtained, D is their degeneracy. We note that $\mathbf{S}^T x_i$ are all negative, so the maximum are just the points which are closest to zero, so these are exactly the support vectors. To continue, for $\tau \rightarrow \infty$ we denote

$$\mathbf{S} \sim E f(\tau) \hat{\mathbf{S}}, \quad (49)$$

where E is some constant, and $f(\tau)$ is some function of t . Without loss of generality, and for compatibility with the results of the main text, we will define E by the equation $E \equiv -\frac{1}{\hat{\mathbf{S}}^T x_m}$. We can now find $f(\tau)$ explicitly using the following arguments: We know that

$$\frac{\partial \|\mathbf{S}\|}{\partial \tau} = \frac{\mathbf{S}^T}{\|\mathbf{S}\|} \frac{\partial \mathbf{S}}{\partial \tau} = -\eta \frac{1}{N} \sum_i e^{\mathbf{S}^T x_i} \frac{\mathbf{S}^T}{\|\mathbf{S}\|} x_i. \quad (50)$$

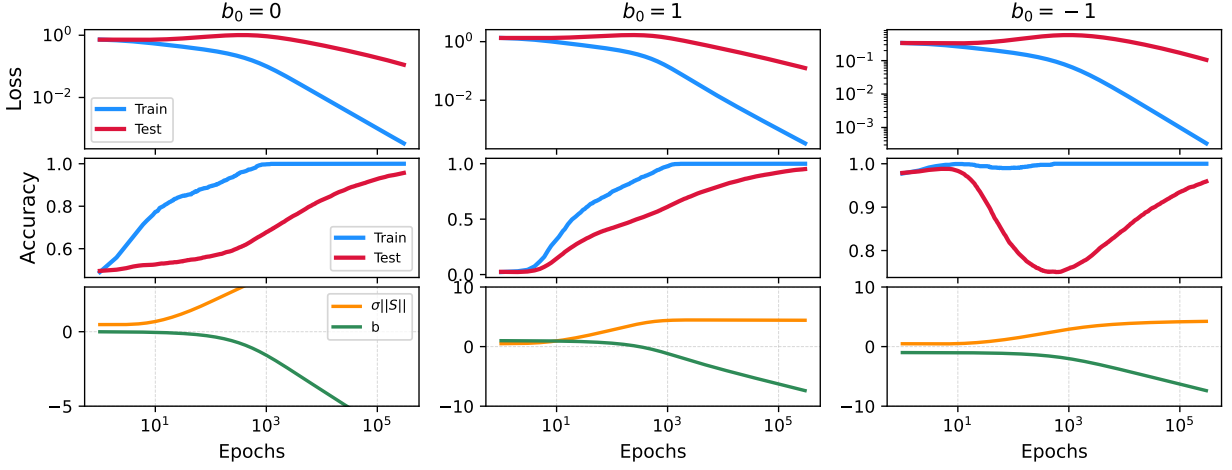


Figure 12: Gradient descent dynamics for $\lambda = 0.48$ and for three different values of b . Except for this, the setup is the same as Fig. 1.

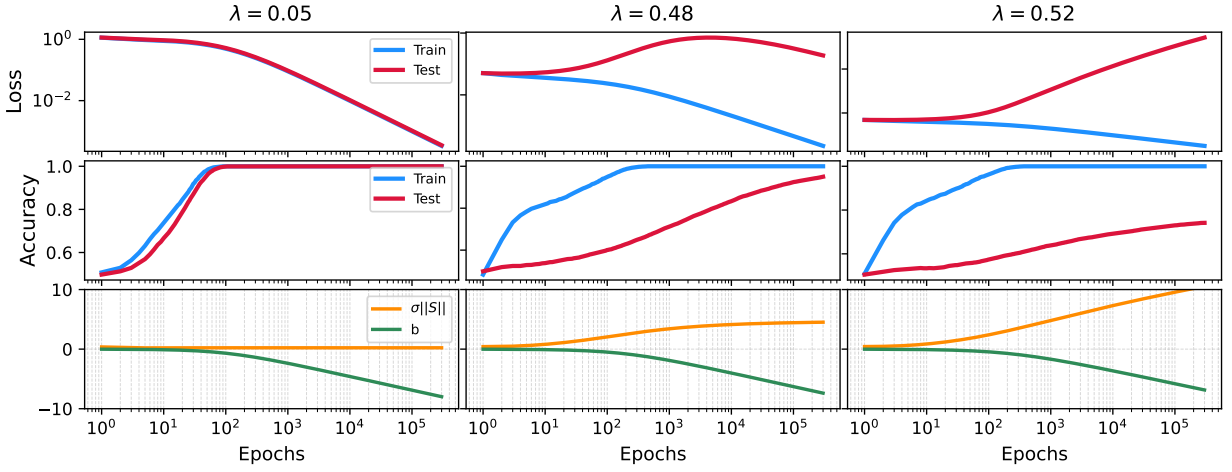


Figure 13: Gradient descent dynamics for a setup which is the same as Fig. 1, but with the exponent loss $\mathcal{L} = \frac{1}{N} \sum_i e^{S^T x_i + b}$. That is, the loss is strictly the exponent loss at any time (and not just converge to the exponent loss at long times, as the CE loss). Clearly, we can see that the behavior of the Grokking is similar.

Using the approximation and comparing with $\frac{\partial \|\mathbf{S}\|}{\partial \tau} = E f'(\tau)$, we get that

$$\eta \frac{D}{N} \frac{1}{E} e^{-f(\tau)} = E f'(\tau). \quad (51)$$

Solving for $f(\tau)$, we get

$$f(\tau) = \log \left[\eta \frac{D}{N} \frac{1}{E^2} \tau + C_1 \right], \quad (52)$$

where C_1 is some constant. Therefore, we get

$$\frac{\partial b}{\partial \tau} \approx -\eta \frac{D}{N} \frac{1}{\eta \frac{D}{N} \frac{1}{E^2} \tau + C_1}. \quad (53)$$

and taking the integral over $d\tau$ we get

$$\beta(\tau) \approx C_2 \left(\eta \frac{D}{N} \frac{1}{E^2} \tilde{t} + C_1 \right)^{-E^2}. \quad (54)$$

Recalling that $\frac{\partial \tau}{\partial t} = e^b$, we can integrate to find:

$$\tau(t) = \frac{1}{\eta \frac{D}{N} \frac{1}{E^2}} \left(\eta \frac{D}{N} \frac{E^2 + 1}{E^2} \right)^{\frac{1}{E^2 + 1}} [C_2 t + C_3]^{\frac{1}{E^2 + 1}} - \frac{1}{\eta \frac{D}{N} \frac{1}{E^2}} C_1. \quad (55)$$

Using $b = \log(\frac{\partial \tau}{\partial t})$, we get for long times that

$$b(t) \approx -\frac{E^2}{E^2 + 1} \log(t). \quad (56)$$

Plugging also $\|\mathbf{S}\| \approx E f(\tau) \approx E \log(\tau)$, we can see that

$$\|\mathbf{S}(t)\| \approx \frac{E}{E^2 + 1} \log(t). \quad (57)$$

Recalling that $E = \frac{1}{M}$, this verifies the result of the main text.

H Supplemental Details of Experiments

In this section, we will provide information regarding the experiments. All of our results are computed in Python, using the standard gradient-descent of the PyTorch library.

We begin by noting that the results of the left panels of Fig. 1 (and all of the results in Section F) can be easily obtained even on a personal laptop. We had only three "large" experiments, which are presented in the right-most column of Fig. 1 (and in Fig. 7):

(1) Calculation of $\|\mathbf{S}_\infty\|$ and $\mathbf{S}^T x_i$ properties of the distribution. The setup is: $N = 2400$, $\sigma = 1$, and $d = 930, 990, 1050, 1086, 1110, 1134, 1152, 1158, 1164, 1170, 1173, 1176, 1179, 1182, 1185, 1188, 1191$, averaged over 15000 different random realizations. This was run in a cluster of servers with 250 Intel(R) Xeon(R) CPU E5-2690 v4 @ 2.60GHz cores with about 9GB RAM per core, which took a few hours to run. The minimization was done using ADAM (any optimizer will work in the inseparable regime).

(2) Calculation of the margin: The setup is: $N = 2400$, $\sigma = 1$, and $d = 1230, 1260, 1290, 1320, 1350, 1380, 1410, 1440, 1470, 1500, 1530, 1560$, averaged over 1000 realizations. Performed on the same cluster, this took only a few hours to run.

(3) The results of the right-middle and right-bottom panels of Fig. 1. The setup is: $N = 400$, and $d = 20, 40, 80, 100, 120, 140, 160, 168, 180, 188, 192, 196, 200, 208, 220, 228, 240, 260, 280, 300, 320, 360$, averaged over 100 realizations. This also took only a few hours to run.